A comparison of extreme mooring loads and response of a spar-buoy wind turbine using conditional waves

A comparison of extreme mooring loads and response of a spar-buoy wind turbine using conditional waves

Aminda M. T. Ripe, David R. Lande-Sudall*
*Western Norway University of Applied Sciences, Inndalsveien 28, 5068 Bergen, Norway
E-mail: dla@hvl.no

Abstract. Three-hour random sea-state evaluations for ultimate limit state design of floating offshore wind installations are time-consuming and prevent the use of high-fidelity numerical methods from being implemented. In this work, three conditional waves, Most-Likely Wave (MLW), Most-Likely Response Wave (MLRW) and Conditional Random Response Wave (CRRW), are experimentally investigated as alternative means to generate statistical extreme responses in surge and mooring line loads of a spar-buoy substructure, with shorter time-series duration compared to a 3-hour JONSWAP sea-state. MLW and MLRW are found to generate the greatest mooring line loads, far greater than the statistical expected maximum from a 3-hour random sea-state. However, MLW is uncorrelated with the substructure's linear transfer function of response, and the MLRW includes no memory effects from a random background sea, indicating possible conservatism in the associated load magnitudes. CRRW is a MLRW embedded within a random background and is found to excite a similar mooring load as the 3-hour sea-state, with memory effects included. CRRW could thus be an appropriate method of generating statistically appropriate load responses within a reduced time-series. However, nonlinear effects on the mooring are not accounted for in any of the methods and will be included in future work.

1. Introduction

As world economies transition towards Net-Zero, the design of floating offshore wind turbine (FOWT) substructures is under rapid development. Compared to traditional design practices used in the oil and gas industry, the strong coupling between the aero-hydro-servo-elastic loads makes FOWT structures highly dynamic. It introduces challenges in accurately modeling their responses and loads using numerical codes [1]. Existing approaches to verifying numerical models are to perform model-scale experiments in wave basins [2], where ultimate-limit state (ULS) design waves are modeled using 3-hour short-term sea-states along an environmental contour of a specified return period [3, 4]. This is time-consuming, both experimentally and numerically, requiring repetition for multiple seed numbers to provide statistical confidence of extreme values.

For bottom fixed structures, ships, and moored floating structures, deterministic focused waves with a height defined by the expected extreme wave height have been studied as an effective means to excite multiple frequency responses simultaneously [5]. An example of such a wave model is the NewWave by Tromans [6]. This wave is focused in both position and time by aligning the phase components in a given sea state. However, this model assumes the extreme responses and loads are correlated at a single extreme event. When memory effects are important, such as for slowly-varying wave drift of moored vessels, a deterministic wave can

be embedded in a random background. Nevertheless, conditioning on wave height or steepness does not account for the structure's response [7, 8].

Presented, is an experimental study on extreme responses and mooring loads for a spar-buoy wind turbine substructure using conditional waves. Three critical wave episodes are computed building on methods from [5, 9, 10]: a focused wave group with the most likely extreme wave height embedded in a random sea called Most Likely Wave (MLW); a wave group conditioned using the complex transfer function of the structure to excite the most likely response (MLRW); a MLRW embedded in a random sea-state (CRRW). For conditioning of the extreme response, data from a 3-hour irregular JONSWAP sea state is used, with H_s and T_p taken from the 1/50 year contour of a site in the Barents Sea.

2. Methodology

2.1. 3-hour random sea-states

Typically, for calculating ultimate limit state design loads, it is required to find the most severe cases from a specified return period of an environmental contour plot of significant wave height, H_s and peak period, T_p, representative of a stationary and ergodic 3-hour sea state [3]. In this case, we obtain statistics for a 1/50 year return period by interpolating between the 1/10 and 1/100 year contours for Block B of the Barents Sea [11], with a water depth of 220 m. A JONSWAP irregular wave spectrum, with peakedness parameter, $\gamma = 3.3$ is assumed applicable for this site. Whilst multiple points along this contour are of interest, we only present results for the 3 hour case in Table 1, since this has the greatest wave power, $P_{wav} \propto H_s^2 T_p$.

In addition to this extreme sea-state, the complex transfer function for the structure is also required. This is obtained experimentally by running a so-called 'white' (or 'pink') noise test, whereby all wave frequencies are excited to an equivalent amplitude. In this case, $H_s = 2$ m is used, which allows non-breaking waves to be generated up to the 0.2 Hz high-frequency cut-off frequency of the wavemaker. Use of a low significant wave height for generating the transfer function means that nonlinear effects are not captured, nor hidden in linearisation. Thus, possible differences with the experiments can be separated from the linear contributions.

Table 1: Spectral sea-state parameters.

Case	H_s [m]	T [s]	S_p[1]
JONSWAP	13	$T_p = 17.3$	0.028
White-noise	2	$33 \geq T \leq 5$	-

[1] where $S_p = 2\pi H_s/(gT_p^2)$ is the steepness parameter defined on T_p [3].

2.2. Most-Likely Wave (MLW)

As discussed, the NewWave model of [6] has been shown to be ineffective for assessing extreme loads for moored floating structures, where memory effects accrued in a random sea may be significant [7]. Following [10], we obtain the Most-Likely Wave, (otherwise known as a Constrained wave [5, 12]) by embedding a NewWave within a random JONSWAP background, defined by the same parameters as in Section 2.1, to attempt to include some of the historical effects.

The NewWave is obtained as the autocorrelation of wave elevation, $\rho(x,t)$ (eqn.(1)), as a function of distance, x, from the wavemaker and time, t, multiplied by the focused wave amplitude, a_{max}.

$$\rho(x,t) = \frac{1}{\sigma^2} \sum_{n=1}^{N} S_{\eta\eta}(\omega_n) \Delta\omega \cos\left[k_n(x - x_{foc}) - \omega_n(t - t_{foc})\right] \tag{1}$$

In Equation (1), σ^2 is the variance of the spectrum, $S_{\eta\eta}(\omega)$, k_n is the wavenumber, $x_{foc} = 185$ m is the full-scale focal distance from the wavemaker (see Section 2.5) and $t_{foc} = 3500$ s the corresponding focal time. For a random background sea elevation, $\eta(x,t)$, with instantaneous amplitude, a_0 and slope, $\dot{a}_0$ at focal time, t_{foc}, the MLW elevation, $\eta_{MLW}(x,t)$ is formulated by subtracting the random background surface elevation at the focal time, before adding in the focused NewWave, as [5, 9]:

$$\eta_{MLW}(x,t) = \eta(x,t) - a_0\rho(x,t) - \dot{a}_0\dot{\rho}(x,t) + a_{max}\rho(x,t) \tag{2}$$

where dot-notation represents the time-derivative.

Assuming that the dominant forcing is still expected to coincide with the focused extreme wave, the total duration for the sea-state can likely be reduced, thus allowing more time-efficient evaluation. In this study, we investigate 1.11 h (4000 s), with a focal time of $t_{foc} = 3500$ s. For a surge period of approx. 150 s (see Section 2.7), this theoretically allows > 20 oscillations, which should be adequate to allow slowly varying oscillations to build up about a mean drift position.

2.3. Most-Likely Response Wave (MLRW)

Most likely response wave (MLRW) is a focused wave group designed to excite a specified response in a specific degree of freedom using a complex transfer function obtained, ideally, from a white noise test. The process used to model the MLRW uses the formulations given by Dietz et al. (2004). Here, the wave is modelled as a vector process, where its definition is formulated using a set of random constrained coefficient vectors $(\overline{V}_n, \overline{W}_n)$ associated with each n-th angular wave frequency component, ω_n. The constrained coefficients are computed based on a Slepian model process [13] using the spectral moments of a chosen sea state (m_0, m_1, m_2), the structure's complex transfer function $H(\omega)$ for a given degree of freedom, y, and the associated phase angles, $\phi_{y,n}$:

$$\overline{V}_n = \frac{a_{y,n}}{m_0 m_2 - m_1^2} \cdot \left[a_y(\omega_n m_1 - m_2)\, \cos\left(\phi_{y,n}\right) - a_y\overline{\omega}_y(\omega_n m_0 - m_1)\, \cos\left(\phi_{y,n}\right)\right] \tag{3}$$

and,

$$\overline{W}_n = \frac{a_{y,n}}{m_0 m_2 - m_1^2} \cdot \left[a_y(\omega_n m_1 - m_2)\, \sin\left(\phi_{y,n}\right) - a_y\overline{\omega}_y(\omega_n m_0 - m_1)\, \sin\left(\phi_{y,n}\right)\right]. \tag{4}$$

The target maximum linear response amplitude, a_y is provided as an input, and the mean response frequency is determined from the spectral moments: $\overline{\omega}_y = \frac{m_1}{m_0}$. The MLRW is conditioned on the linear response of the structure where the coefficient $a_{y,n}$ is determined using the wave spectrum, $S_{\eta\eta}(\omega_n)$, and the structure's transfer function, given as:

$$a_{y,n} = |H(\omega_n)| \sqrt{S_{\eta\eta}(\omega_n)\, \Delta\omega_n}\,. \tag{5}$$

Finally, the MLRW surface elevation as a function of position, x, and time, t, is given by:

$$\eta_{MLRW}\,(x,t) = \sum_{n=1}^{N} a_{y,n}\left[\overline{V}_n\, \cos\left(k_n x - \omega_n t\right) + \overline{W}_n\, \sin\left(k_n x - \omega_n t\right)\right] \tag{6}$$

where the wave number, k_n is found using the linear dispersion relation.

2.4. Conditional Random Response Wave (CRRW)

A MLRW with a random background sea is called a Conditional Random Response Wave (CRRW). This wave definition is simply computed by adding the wave amplitudes of a given random background sea, $\eta(x,t)$, and MLRW surface elevations, $\eta_{MLRW}(x,t)$, as:

$$\eta_{CRRW}\,(x,t) = \eta(x,t) + \eta_{MLRW}(x,t). \tag{7}$$

2.5. Experimental apparatus

Physical experiments on a 1:100 model-scale spar buoy wind turbine substructure, supporting a 15 MW wind turbine [14], have been conducted in the 220 m deep (full-scale) MarinLab towing tank at the Western Norway University of Applied Sciences (HVL). The towing tank has a total length of 50 m, width of 3 m and is equipped with a six-flap wavemaker, with force-feedback control and generates waves following second-order wavemaker theory [15]. A Qualisys motion capture system, with four cameras is installed above the tank to record the floater's motions in six degrees of freedom at 100 Hz sampling frequency. Six resistance-type wave gauges record the surface elevation at 128 Hz, and their positions are shown in Figure 1(a). Wave gauge #4 is aligned to one side of the model's flotation centre, at 18.5 m (model-scale) from the wavemaker.

The overall full-scale dimensions of the spar buoy are illustrated in Figure 1(b). The substructure is designed with a heave plate of diameter 20 m. The floater is moored with a light mooring system consisting of three lines connected to the floater at the still-water level and three individual load cells with a capacity of 30 N to measure forces in the tension-direction. The upstream load cell (LC1) is aligned with the incoming waves along the tank centreline, with the other two load cells (LC2 and LC3) spread at approximately 120° towards the tank walls.

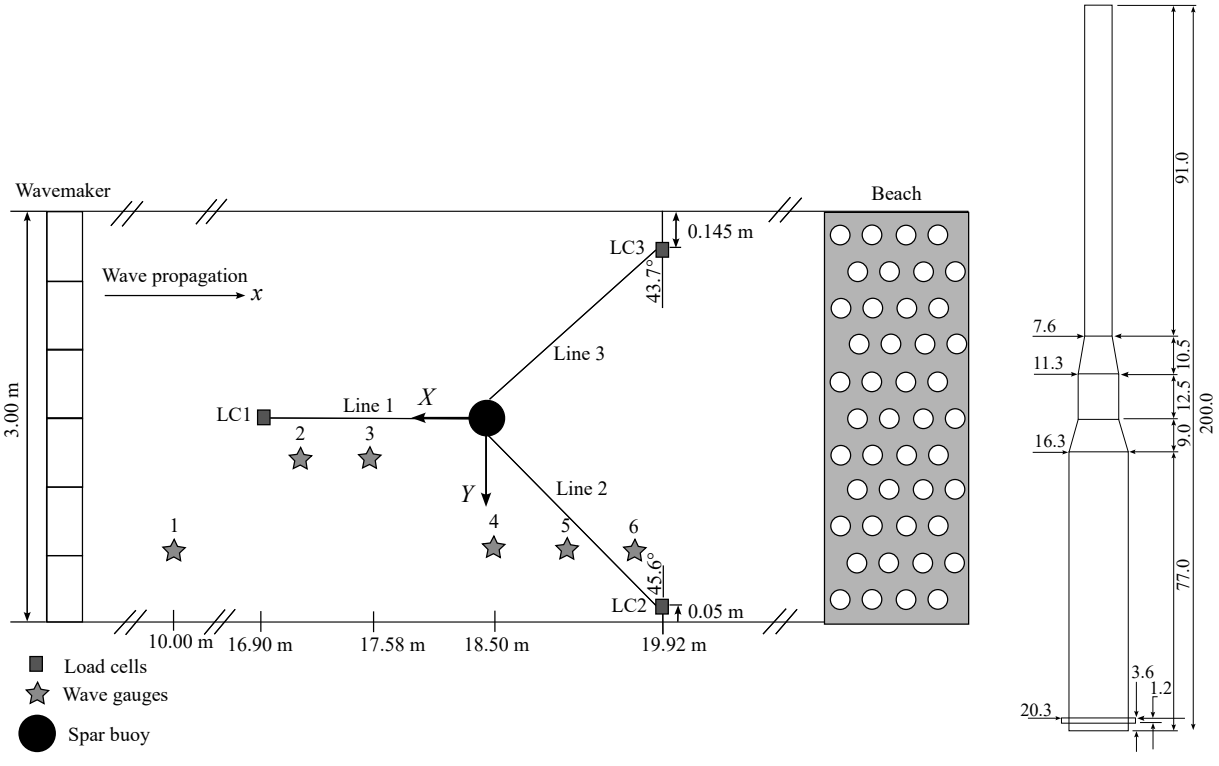

Figure 1: (a) Schematic diagram showing model rest-position in the MarinLab towing tank with wave gauges and mooring arrangement, and (b) full-scale dimensions of the spar-buoy floater.

Table 2: Overall structural properties of the full-scale spar-buoy. Scale factor, $\lambda = 100$.

Particular	Dimensions
Total mass (dry), tonnes	18,123.7
RNA mass, tonnes	989.8
Draught, m	90
Mass centre over keel, m	[0,0,35]

2.6. Calibration and repeatability

The load cells are linearly calibrated, with a maximum hysteresis of less than 0.1% of the full-scale range. Similarly, the wave gauges are linearly calibrated over a 35 cm range, with maximum uncertainty of less than 0.1% of this range. Each wave spectrum is calibrated using a frequency-dependent gain correction. The calibrated 3-hour JONSWAP sea state had a measured $H_s = 12.84$ m, which is within 1.2% of the target. The white-noise spectrum gave a 6% error on the target $H_s = 2.00$ m, however, this is expected, given the difficulty in obtaining small amplitudes uniformly across the spectrum.

For the conditional waves, the interest is in reproducing an exact time-series of wave elevation, thus these waves are applied as a time-series of elevation. In practice, this is not straightforward, since tank reflections are difficult to control in the time-domain, as well as the actual focus position being affected by nonlinear wave-wave interactions [16]. For the MLW, frequency-dependent linear gain corrections are obtained in the same manner as the for the JONSWAP and white-noise spectra, and are applied to the frequency components before transforming back into a new target time-series. For the MLRW and CRRW, the gains are also calculated as the ratio between measured and target spectra, and then applied to each the background sea spectrum and MLRW components separately, prior to their summation in Equation (7) for CRRW.

Figure 2 demonstrates the excellent repeatability of the time-series between three repeat measurements conducted on the MLW and MLRW, with only a single measurement of the calibrated CRRW taken. Despite some discrepancies with the theoretical profiles, good agreement with each of the target focus amplitudes is achieved. Since differences in the low frequency content could contribute to significant differences in response around the surge resonant frequency, the power spectrum of the low-pass filtered undisturbed wave elevation ($f < 0.03$ Hz) is also shown. In general, all repetitions have similar low frequency spectral energy, although one of the MLW repeats seems to have a slight frequency shift. For the MLRW, which is essentially just a focused wave, there is little chance for significant discrepancies in reflections to build up.

2.7. Decay tests

Decay tests of the lightly-moored spar-buoy are conducted for a range of degrees of freedom. The results for natural period, $T_0 = 2\pi/\omega_0$, and linear damping ratio, ζ are given in Table 3 and are obtained by least-squares fitting of an exponential decay function of the form (Eqn. (8)):

$$y(t) = A \exp\left(-\zeta\omega_0 t\right) \sin\left[\sqrt{1-\zeta^2}\omega_0 t + B\right] \tag{8}$$

Table 3: Spar-buoy undamped eigenperiods, T_0 and corresponding linear damping factors, ζ, for a range of degrees of freedom (DOF), obtained via decay tests.

DOF	T_0, s	ζ, [-]
Surge, X	149.3	0.07
Heave, Z	27.7	0.016
Pitch, Θ	35.7	0.017

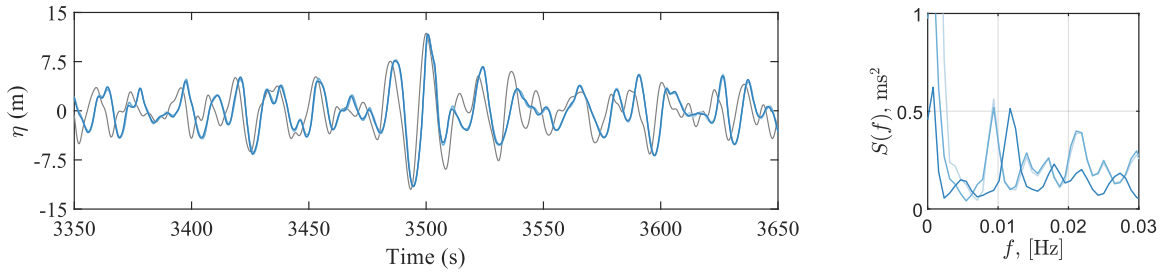

(a) MLW

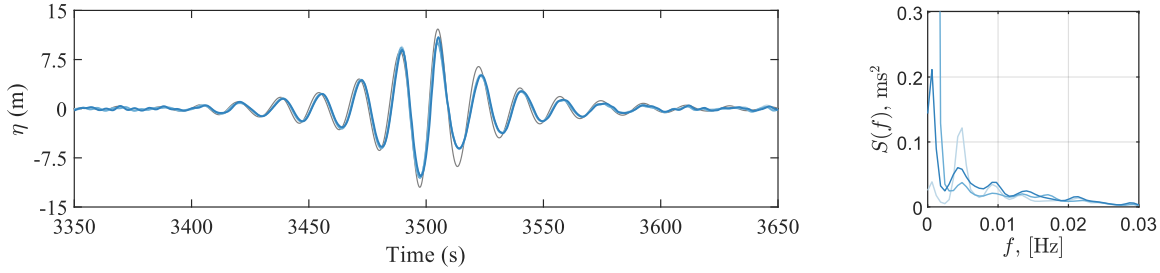

(b) MLRW

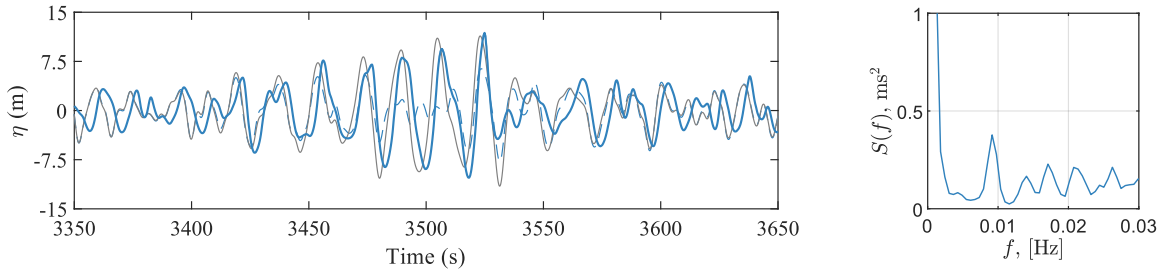

(c) CRRW

Figure 2: Left: surface elevation, $\eta(t)$ around focus time, $t_{foc} = 3500$ s and Right: corresponding power spectral density of the low frequency wave elevation ($f < 0.03$ Hz) for theoretical profiles, — and three repeat measurements, —,—,—, of (a) MLW, (b) MLRW, and (c) CRRW. Note, CRRW only had a single measurement of the calibrated wave. Theoretical JONSWAP background, - - -.

3. Results

3.1. White-noise test

The complex transfer function, $H(\omega)$ for the structure is obtained from the white noise test as the ratio of cross power spectrum, $S_{\eta y}(\omega)$ of response, y, with input, η, to auto power spectrum of input, $S_{\eta\eta}(\omega)$, with corresponding phase angle, ϕ:

$$H(\omega) = \frac{S_{\eta y}(\omega)}{S_{\eta\eta}(\omega)} \tag{9}$$

$$\phi(\omega) = \arctan\left(\frac{a}{b}\right) \tag{10}$$

where a and b are the real and imaginary components of $H(\omega)$, respectively.

The corresponding Response Amplitude Operators, RAOs ($|H(\omega)|$), defined between the wavemaker cutoff frequencies of 0.03 Hz and 0.2 Hz, are shown for surge, X, heave, Z, pitch, Θ and mooring line loads in Figure 3. Noticeable, is a surge-pitch coupling typical of spar-buoys, and there is a clear correlation between load response and the pitch eigenperiod around 28 s. Here, we focus on the response in surge, though transfer functions can be obtained for any of the desired degrees of freedom.

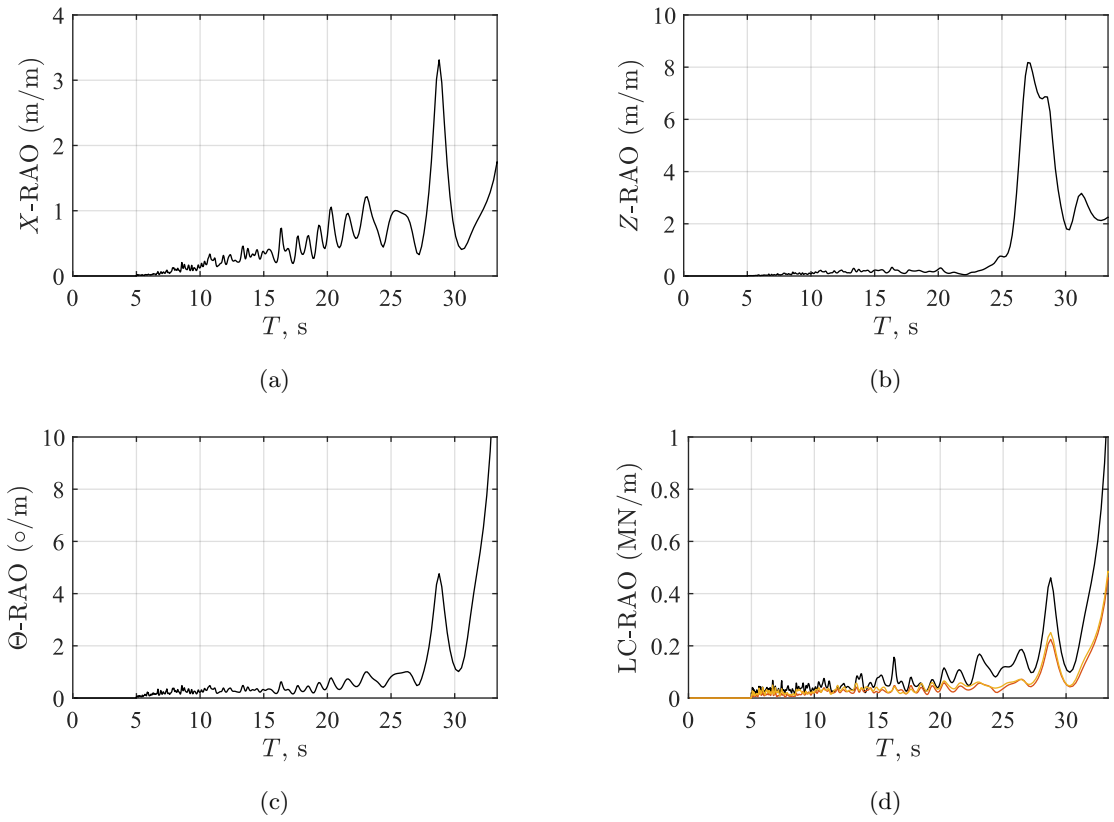

Figure 3: Response Amplitude Operator (RAO) curves for (a) surge, (b) heave, (c) pitch, and (d) load cells LC1(—), LC2(—) and LC3(—) obtained from a white-noise test.

3.2. 3-hour extreme response

From the 3-hr JONSWAP wave spectrum and response spectra in surge, pitch and mooring load, the statistical maxima of wave amplitude ($a_{max} = H_{max}/2$), and other responses are calculated from the moments, m_0, m_1 of their respective spectra (Table 4). It is assumed that the maxima of both wave height and response are Rayleigh distributed, such that they may be obtained as Eqn.(11) for $N = 10800 \times m_0/m_1$ number of waves [17], and where χ_{max} represents a statistical maximum amplitude. This provides a suitable estimate of the extreme response for which to target. Nevertheless, this assumption may not strictly follow, especially for surge, where low frequency oscillations occur outside of the wave frequency range. Thus for surge, the absolute maximum response amplitude recorded in the time-series is also reported and it is this value, $X_0 = 7.4$ m that is used as the target input for the conditional waves.

$$\chi_{max} = \frac{1}{2}\sqrt{m_0 \ln(N)} \tag{11}$$

It should be noted that the statistical maximum values are independent of each other, and do not consider their combined probability, e.g. of the maximum wave amplitude, a_{max}, occurring with local up-crossing period, T_z, or of both pitch and surge responses taking a maximum which also could be relevant given their strong coupling.

3.3. Comparison of MLW, MLRW and CRRW maximum responses

Figure 4(a)-(f) show the time-series surge and mooring line responses from load cell LC1, as measured at the focal time in each of the MLW, MLRW and CRRW tests. Presumably due to slow-drift of the vessel downstream of the focus position, x_{foc}, and nonlinear wave-wave interactions, the maximum surge and corresponding load responses occur just prior to the focal time, $t_{foc} = 3500$ s. Since we are interested in the effect of the local wave group around the focus time, we obtain the maximum response values at the point in time where maximum mooring load occurs,, as opposed to the response at exactly $t = t_{foc}$, or at the maximum wave amplitude, a_{max}. Maximum force response coincides with maximum surge response, which whilst moving nearer the load cell should slacken the line, the corresponding pitch response is also a maximum negative, hence causing the high tension. The absolute values of surge, pitch and mooring response are summarised in Table 4. Three repeats of each MLW, MLRW and CRRW found the relative root-mean-squared error in mooring loads to never exceed more than 4% of the peak load induced by each wave-type, apart from for one repetition of MLRW which was 8.6%.

Table 4: Global responses in surge, X, pitch, Θ, and tension in load cell 1, F_{LC1}, measured at times, $t_{meas.}$ and marked with ○ in Figures 4(a)-(f), for the MLW, MLRW and CRRW, with maximum undisturbed wave amplitudes, a_{max}. Statistical maxima of the 3-hr JONSWAP, obtained by Eqn. (11), are given for comparison. All amplitudes are calculated as half the local peak-to-trough value.

Case	a_{max}, m	$t_{meas.}$, s	X, m	Θ, °	F_{LC1}, kN
JONSWAP	11.3	0 - 4000	5.2	4.6	1392
MLW	11.3	3487	3.7	3.4	1663
MLRW	10.6	3492	5.0	4.1	1618
CRRW	9.7	3489	4.9	3.7	1311

Each of the MLW and MLRW cases give mooring loads approximately 16-19% greater than the statistical maximum from the 3 hr JONSWAP. For MLW, the local wave amplitude is identical to the statistical maximum, as expected from the theory. However, since the wave takes no consideration of the floater's transfer function, the surge response is uncorrelated and therefore much lower than the statistical maximum from the 3 hr JONSWAP. At the same time, the JONSWAP maximum mooring load is smaller than for the MLW, because the JONSWAP result is only statistical and uncorrelated with the occurrence of maximum wave height or surge response. This highlights a difficulty in using a MLW in extreme response analysis, as despite the wave being successful in exciting an extreme load, the response values obtained have no correlation to the underlying statistical response of the 3hr sea-state. The MLRW gives a similar mooring load to the MLW, with $\sim 5.5\%$ reduction in wave amplitude, which is likely within the calibration uncertainty of the input wave calibration. Instead, the MLRW surge response is closer to the statistical maximum from the JONSWAP spectrum, but still short of the target input, $X_0 = 7.4$ m. The CRRW attains a similar surge response to the MLRW, as expected, given that the CRRW is just a MLRW embedded on a random background. Whilst the maximum mooring load is much less than those obtained from the MLW and MLRW, it is very similar ($< 4\%$) to the statistical maximum of the JONSWAP spectrum, suggesting that the CRRW could be more representative in re-creating the load conditions of the 3hr sea-state.

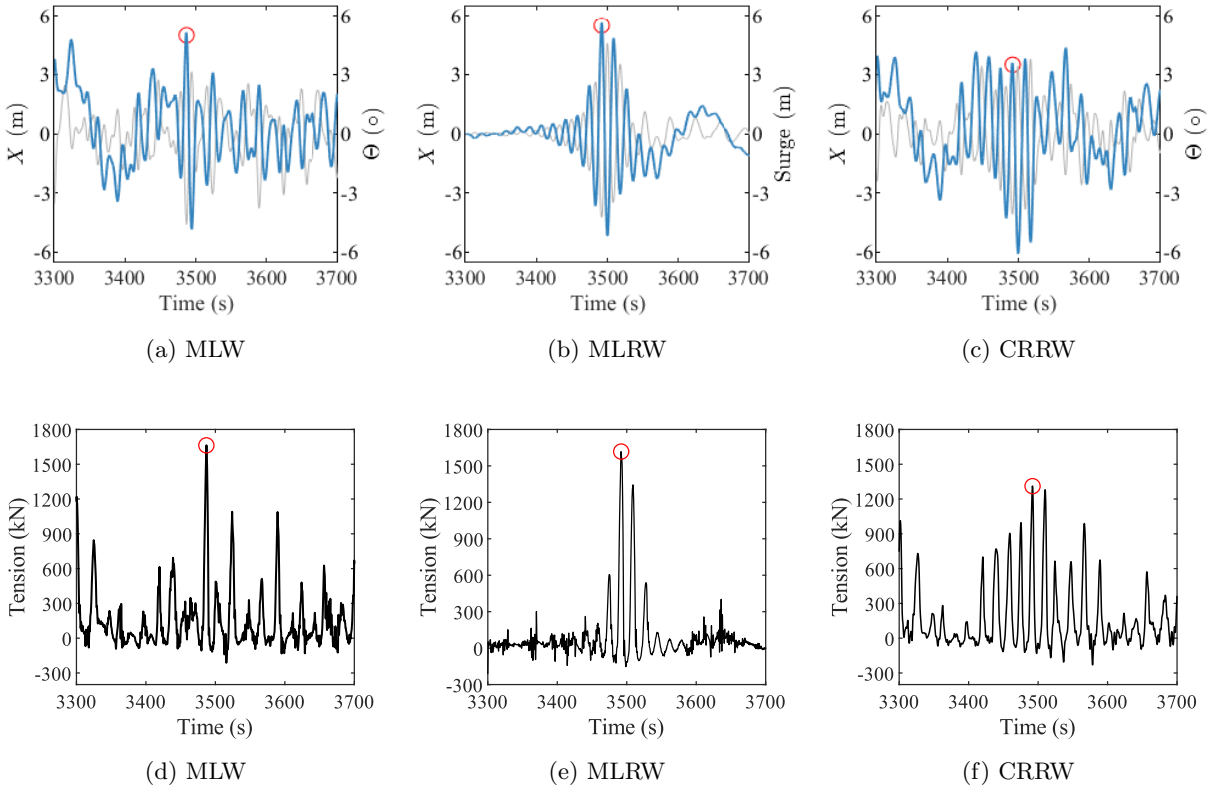

(a) MLW (b) MLRW (c) CRRW

(d) MLW (e) MLRW (f) CRRW

Figure 4: (Top) response in surge, X (—) and pitch, Θ (—), and (Bottom) response in tension, F_{LC1} in LC1 (—) for MLW (left), MLRW (centre) and CRRW (right). Maximum values (○) given in Table 4.

However, CRRW still does not generate the expected maximum wave height, which is possibly due to the way the superposition relation of Eq. (7) is applied.

It should be noted that all of these waves, with linear assumptions, have been generated for a focus location at the model rest-position and therefore do not account for mean or slow-varying drift of the model. The problem is further compounded given that nonlinear wave-wave interaction causes movement of the focal location away from the linear target [16]. This was casually observed in the wave gauge signals for the MLW, where the wave amplitude was around 15% greater at wave gauge #6 than at wave gauge #4, and an asymmetry about the crest suggested that the focal location would actually occur even further downstream.

4. Conclusions and future work

This work has investigated the use of conditional waves as an efficient method of assessing ultimate design loads associated with extreme waves, by reducing the time required for experimental measurement and in future, for numerical comparisons. The most-likely wave (MLW) generated the expected maximum wave height for a 3-hour JONSWAP sea-state, but the corresponding induced mooring load was far greater than the extreme value predicted from a 3 hour JONSWAP random sea-state, suggesting the return-period was greater than the 1/50 year contour that was used as input and hence an overly conservative design load. The most-likely response wave (MLRW) excited a similar level of response as the MLW. This case highlights

the importance of considering the device's transfer function in selection of design waves. In contrast, whilst the conditional random response wave (CRRW) experienced a similar peak response as MLRW, it had a load response that was closest to the maximum expected from the 3 hour JONSWAP, suggesting that the inclusion of historical time-series effects are important for correct generation of design loads. In all cases, linear wave theory is assumed as the basis for the conditional waves, however this neglects the effect of low-frequency forcing and wave drift which is significant for slack-moored vessels. Work is on-going to include second-order effects and thus exercise greater control over the design of shorter, representative time-series extreme waves that can be more readily compared with numerical simulations than for full 3hr sea-state computations. Furthermore, an assessment on how short the time-series can be reduced by for accurate reproduction of the structure's global response needs to be evaluated.

References

[1] A. N. Robertson, S. Gueydon *et al.*, "OC6 Phase I: Investigating the underprediction of low-frequency hydrodynamic loads and responses of a floating wind turbine," *Journal of Physics: Conference Series*, vol. 1618, no. 3, p. 032033, Sep. 2020.
[2] A. N. Robertson, F. Wendt *et al.*, "OC5 Project Phase II: Validation of Global Loads of the DeepCwind Floating Semisubmersible Wind Turbine," *Energy Procedia*, vol. 137, pp. 38–57, Oct. 2017.
[3] DNVGL, *DNV-RP-C205 Environmental Conditions and Environmental Loads*, 2014.
[4] S. R. Winterstein, T. C. Ude *et al.*, "Environmental parameters for extreme response: Inverse FORM with omission factors," in *ICOSSAR-93*, Innsbruck, Austria, 1993, pp. 9–13.
[5] M. Cassidy, R. Eatock Taylor, and G. Houlsby, "Analysis of jack-up units using a Constrained NewWave methodology," *Applied Ocean Research*, vol. 23, no. 4, pp. 221–234, Aug. 2001.
[6] P. S. Tromans, A. R. Anatruk, and P. Hagemeijer, "New Model for the Kinematics of Large Ocean Waves Application as a Design Wave," *Proceedings of the First International Offshore and Polar Engineering Conference*, vol. 8, no. August, pp. 64–71, 1991, iSBN: 0962610488.
[7] M. Hann, D. Greaves *et al.*, "Use of constrained focused waves to measure extreme loading of a taut moored floating wave energy converter," *Ocean Engineering*, vol. 148, no. October 2017, pp. 33–42, 2018, publisher: Elsevier Ltd.
[8] L. Adegeest, A. Braathen, and T. Vade, "Evaluation of methods for estimation of extreme nonlinear ship responses based on numerical simulations and model tests," in *Twenty-Second Symposium on Naval Hydrodynamics*. Washington D.C.: National Academies Press, Aug. 1998.
[9] J. S. Dietz, "Application of Conditional Waves as Critical Wave Episodes for Extreme Loads on Marine Structures," Ph.D. dissertation, Technical University of Denmark, 2004, issue: July ISBN: 8789502434.
[10] P. H. Taylor, P. Jonathan, and L. Harland, "Time Domain Simulation of Jack-up Dynamics With the Extremes of a Gaussian Process," in *Proceedings of the 14th International Conference on Ocean, Offshore and Arctic Engineering (OMAE)*, 1997.
[11] Statoil, "Barents East blocks Metocean Design Basis," BaSEC, Tech. Rep. ME2015_005, Nov. 2015.
[12] "EN IEC 61400-3-1:2019 Wind energy generation systems. design requirements for fixed offshore wind turbines," 2019.
[13] O. Ditlevsen and N. J. Tarp-Johansen, "Slepian modeling as a computational method in random vibration analysis of hysteretic structures," p. 13, 1998.
[14] E. Gaertner, J. Rinker *et al.*, *Definition of the IEA 15-Megawatt Offshore Reference Wind Turbine*. National Renewable Energy Laboratory (NREL), 2020.
[15] J. Spinneken and C. Swan, "Second-order wave maker theory using force-feedback control. Part I: A new theory for regular wave generation," *Ocean Engineering*, vol. 36, no. 8, pp. 539–548, Jun. 2009.
[16] T. Baldock, C. Swan, and P. Taylor, "A laboratory study of nonlinear surface waves on water," *Phil. Trans. R. Soc. A.*, vol. 354, pp. 649–676, 1996.
[17] M. S. Longuet-Higgins, "On the Statistical Distribution of the Heights of Sea Waves," *Journal of Marine Research*, vol. 11, no. 5, pp. 245–266, 1952.